**Article:**
Arkawazi, HDJ orcid.org/0000-0002-6973-6927, Clowes, R orcid.org/0009-0002-4686-2119, Cooper, AI orcid.org/0000-0003-0201-1021 et al. (4 more authors) (2019) Complex phase behaviour and structural transformations of metal-organic frameworks with mixed rigid and flexible bridging ligands. Chemistry - A European Journal, 25 (5). pp. 1353-1362. ISSN 0947-6539

https://doi.org/10.1002/chem.201805028

# Complex phase behaviour and structural transformations of metal-organic frameworks with mixed rigid and flexible bridging ligands.

Hayder D. J. Arkawazi,[a] Rob Clowes,[b] Andrew I. Cooper,[b] Takumi Konno,[c] Naoto Kuwamura,[c] Christopher M. Pask[a] and Michaele J. Hardie*[a]

**Abstract:** Two new heteroleptic metal-organic framework materials show strong adsorption of $H_2$ and ethanol. $[Co_2(L1)(bdc)_2]$, where L1 = $N^1$,$N^4$-bis(4-pyridinylmethyl)-2,5-dimethylbenzene-1,4-diamine and bdc is benzene-1,4-dicarboxylate, has a twofold interpenetrating pillared layer structure with **pcu** topology. It has a stepped, hysteretic EtOH adsorption that can be related to complicated phase and structural transformation behaviour that occurs on de-solvation and re-solvation, including major conformational changes to the geometry of the flexible L1 ligand. $[Co_2(L1)(bpdc)_2]$, where bpdc = biphenyl-4,4'-dicarboxylate, has a unique six-connected self-catenating framework structure. Solvation changes occur without significant structural change and a partially-hydrolysed material binds its own decomposition products as guests.

## Introduction

Metal-organic frameworks (MOFs) and porous coordination polymers (PCPs) are porous materials constructed from metal nodes or clusters and bridging organic ligands.[1] They have a well-ordered polymeric 2D or 3D coordination framework structure, leading to channels or pores where guest molecules can be bound. Guest binding ability leads to a range of applications including gas/substrate storage,[2] catalysis,[3] and drug delivery.[4] The behaviour of MOF/PCPs is quite distinct from other classes of porous materials such as inorganic zeolites as they may be amenable to post-construction chemical modification [5] or exhibit structural dynamism,[6-11] the latter often associated with changes to guest inclusion. Indeed, the ability of coordination polymers to undergo significant structural changes on exchange of guest solvent was one of their first reported properties.[7] Dynamic structural behaviour within MOFs/CPs includes changes to metal coordination mode, rotations of ligand groups, 'breathing' where the entire framework undergoes a concertina-like motion,[8,10] and 'gate-opening' usually associated with relative shifting of two or more interpenetrating frameworks with respect to each other to open pores or channels within the material.[9]

Some of the most commonly employed bridging ligands are carboxylates and pyridyl-donor ligands. These can be combined to form heteroleptic (mixed ligand) MOFs,[12] and this allows for both structural variations and is a mechanism for introducing different chemical functionality into the material. Here we report new Co(II) MOF materials from the new flexible ligand $N^1$,$N^4$-bis(4-pyridinylmethyl)-2,5-dimethylbenzene-1,4-diamine (L1) combined with rigid linear di-carboxylates. This includes a new topologically-complex self-catenating structural type. There are few previous examples of carboxylate/bis-pyridyl MOF-type materials with a similar diamine [13] or diimine ligands,[14] although examples with diamides are more known.[15] The MOFs reported here have good sorption properties for $H_2$ and EtOH, with one showing hysteretic EtOH adsorption, which can be related to its highly complicated phase and structural transformation behaviour.

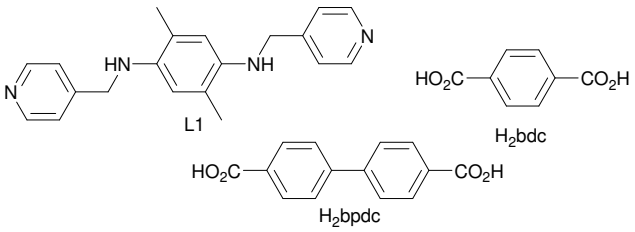


## Results and Discussion

Ligand $N^1$,$N^4$-bis(4-pyridinylmethyl)-2,5-dimethylbenzene-1,4-diamine (L1) was synthesised via reaction of 2,5-dimethylbenzene-1,4-diamine with 4-pyridinecarboxaldehyde to give the diimine which was subsequently reduced using $NaBH_4$. X-Ray structures of L1 and its imine precursor are given in supporting information (Figs. S17, S18). Solvothermal reaction of L1 with 1,4-benzenedicarboxylic acid ($H_2bdc$), and $Co(NO_3)_2$ at 115 °C in N,N-dimethylformamide (DMF) for 24 or 48 hrs gives compound $[Co_2(L1)(bdc)_2]\cdot n(DMF)$ **1** as block red crystals. On some occasions a second product $[Co_2(L1)_2(bdc)_2]\cdot H_2O$ **2** was also observed as orange microcrystals. Compound **2** does not form if freshly prepared L1 is used. The morphologies of the two products were quite distinct and orange microcrystals of **2** could be easily separated from large red block crystals of **1**, Fig. S1 (supporting information). Similar reaction using the precursor diimine rather than L1 did not give crystalline material. Compound **1** shows complicated phase behaviour with two dominant phases

[a] Mr H. D. J. Arkawazi, Dr C. M. Pask, Prof M. J. Hardie
School of Chemistry
University of Leeds
Leeds, LS2 9JT, UK
E-mail: m.j.hardie@leeds.ac.uk
[b] Dr R. Clowes, Prof A. I. Cooper
Department of Chemistry
University of Liverpool
Liverpool L69 7ZD, UK
[c] Prof T. Konno, Dr N. Kuwamura
Department of Chemistry, Graduate School of Science
Osaka University
Toyonaka, Osaka 560-0043, Japan

Supporting information for this article is given via a link at the end of the document.

$Co(NO_3)_2$ + $H_2$bdc + L1

DMF | 115°C

$[Co_2(L1)(bdc)_2].n(DMF)$ **1**

Mixed phase material:

**α-1(L)** - dominant polymorph (ca. 44.5 %)

**β-1(S)** - dominant polymorph (ca. 48%)

**γ-1(L)** - minor polymorph (ca. 3 %)

**δ-1(L)** - minor polymorph (ca. 4.5 %)

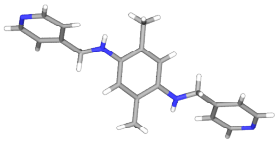

L = linear L1 conformation

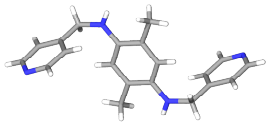

S = bent L1 conformation

acetone

vacuum at rT

Poorly xtalline bulk, can isolate:

$[Co_2(L1)(bdc)_2]$ **ε-1(L)**

$[Co_2(L1)(bdc)_2].^1/_2(DMF)(COMe_2)$ **β-1(S)$^{ace}$**

EtOH

Mixed phases, can isolate:

$[Co_2(L1)(bdc)_2].n(EtOH)$ **γ-1(L)$^{EtOH}$**

$[Co_2(L1)(bdc)_2].2(EtOH)$ **ζ-1(S)$^{EtOH}$**

**Scheme 1.** Phase behaviour of as-synthesised compound **1** and on de-solvation and EtOH treatment. 107 crystals from five different batches were examined and 92 found suitable for complete structure determination or gave reliable unit cell measurements. The approximate distributions of phases from those 92 crystals is given.

found, **α-1(L)** and **β-1(S)** – where L (linear) and S designate the conformation adopted by the L1 ligand - alongside minor amounts of closely related phases **γ-1(L)** and/or **δ-1(L)**, Scheme 1. Multiple unit cell measurements on different batches of **1** indicate roughly equal amounts of **α-1(L)** and **β-1(S)** being formed from a 1:1:1 mixture of L1:$H_2$bdc:$Co(NO_3)_2$ heated for 24 hrs or 1:2:2 mixture of heated for 48 hrs, while a 1:2:2 mix heated for 24 hrs was dominated by **α-1(L)**, and 1:1:1 for 48 hrs by **β-1(S)**. All phases of **1** have the same network topology and degree of interpenetration, and have analogous metal coordination behaviour.

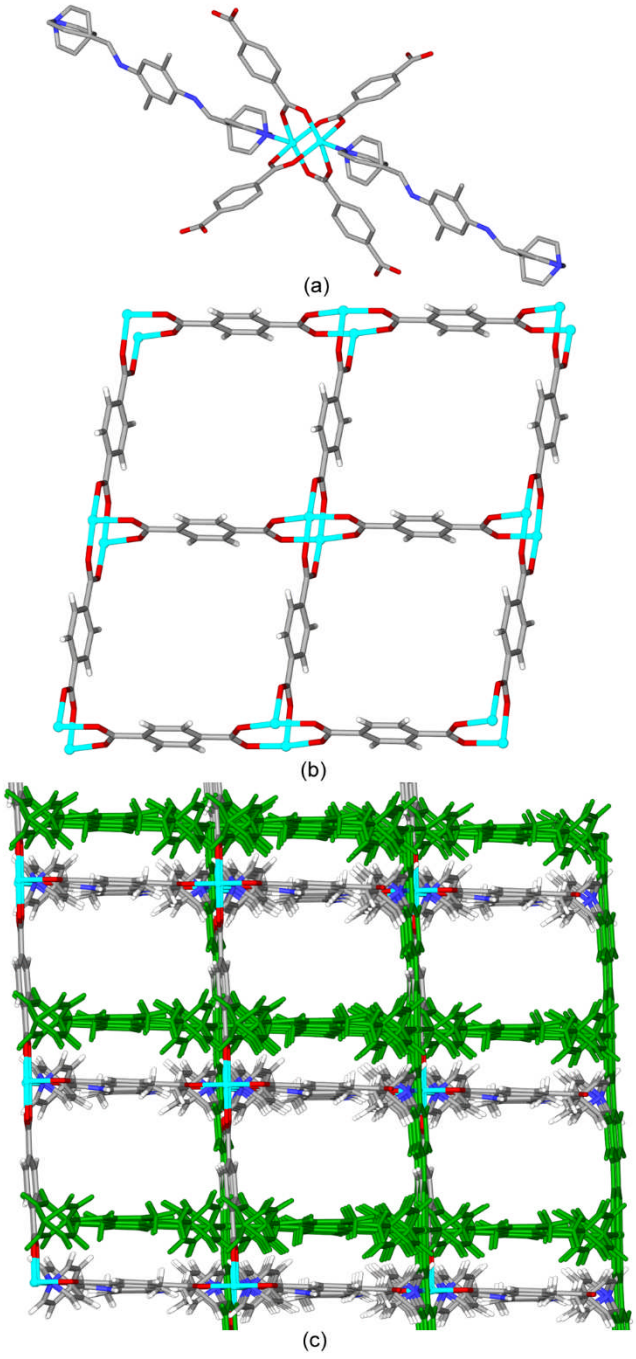


**Figure 1.** Crystal structure of $[Co_2(L1)(bdc)_2]$·n(DMF) **α-1(L)**. (a) Co(II) coordination environment; (b) square grid [Co(bdc)] network; (c) twofold interpenetrating MOF structure viewed down *c* axis which one network shown in green.

$[Co_2(L1)(bdc)_2]$·n(DMF) **α-1(L)** is a MOF material with carboxylate groups bridging between two Co(II) centres at Co-O distances 2.011(5) – 2.083(5) Å. An asymmetric dimeric $Co_2(O_2CR)_4$ paddlewheel motif is formed, Fig 1a. Each $bdc^{2-}$ bridges between two $Co_2$ paddlewheel dimers to form a 2D grid

of **sql** cluster topology, Fig. 1b. The Co(II) centres have square pyramidal geometry and are also bound by a pyridyl of L1 in axial positions at Co-N distances 2.050(6) and 2.059(6) Å. There is one crystallographically distinct L1 ligand which adopts a linear conformation and where each pyridyl group is disordered. The L1 ligand bridges between the **sql** layers thus forming an overall 3D network with **pcu** cluster topology. This is a known structural type for MOFs occurring with $M_2(O_2CR)_4$ paddlewheel clusters and bridging pyridyls.[11,16] and the parent structure is that of DMOF-1 which occurs as a single framework with bridging 1,4-diazabicyclo[2.2.2]octane] ligands.[10]

There are two such **pcu** networks in **α-1(L)** forming an interpenetrated lattice, Fig. 1c, however the second network is not centred with respect to the first, with face-to-face π–π stacking interactions between L1-phenyl groups of one network and bdc-phenyl groups of another at ring centroid separations of 3.62 Å. The lattice has rectangular-shaped channels and 3D solvent accessible void space comprising 39.6 % (1.2 Å probe) of the unit cell volume. DMF solvent could not be located in the structure due to disorder.

The second phase that occurs in significant proportions, $[Co_2(L1)(bdc)_2]\cdot 2(DMF)$ **β-1(S)**, also features a twofold interpenetrating **pcu** cluster topology, and with $Co_2(O_2CR)_4$ paddlewheel moieties. The two **pcu** networks within the material however are not structurally the same, each with a quite different Co environment. The coordination environments around each type of $Co_2(O_2CR)_4$ paddlewheel are shown in Fig. 2. One paddlewheel (Co2) is considerably more skewed from nominal $C_4$-symmetry with three Co-O distances in the range 2.029(1) – 2.038(2) and one much longer at 2.217(2) Å. Whereas for the other (Co1) all Co-O distances are in the range 2.023(2) – 2.062(2) Å. Unlike for **α-1(L)** the L1 ligand adopts an S-conformation with angles between mean planes of pyridyl and phenyl rings of 81.2° and 88.8° for the two L1 ligands respectively. This leads to a much reduced distance between the **sql**-type $[Co(bdc)_2]$ layers (taken as closest Co···Co distance) of ca. 15.9 Å compared with 19.6 Å for **α-1(L)**. As can be seen in Fig. 2a, the orientation of the bridging L1 ligands with respect to the paddlewheel motif is also quite distinct for the two types of $[Co_2(L1)(bdc)_2]$ network. This results in two **pcu** networks with different conformations, shown viewed down the *c* axis in Fig. 2b. There are no face-to-face π–π stacking interactions between the networks, and the NH groups of each L1 are directed towards $bdc^{2-}$ ligands of the other network though not at distances suggesting non-classical hydrogen bonds. Two DMF solvent molecules were located in the structure which are contained within channels and do not have strong interactions with the MOF framework, Fig. S24. Excluding these DMF molecules, the **β-1(S)** phase has 1D solvent-accessible void spaces at a total of ca. 34 % of the unit cell (1.2 Å probe). This is however a much more sterically-restricted space than the 3D void space seen in **α-1(L)**.

Compound $[Co_2(L1)(bdc)_2]\cdot(H_2O)\cdot(DMF)$ **γ-1(L)** is very similar to **α-1(L)** but with two crystallographically distinct $Co_2(O_2CR)_4$ paddlewheel moieties. One of these is significantly skewed (Co1, Fig. 3a) with one carboxylate bridging between the two Co(II) centres at Co-O distances 2.021(4) and 2.038(5) Å,

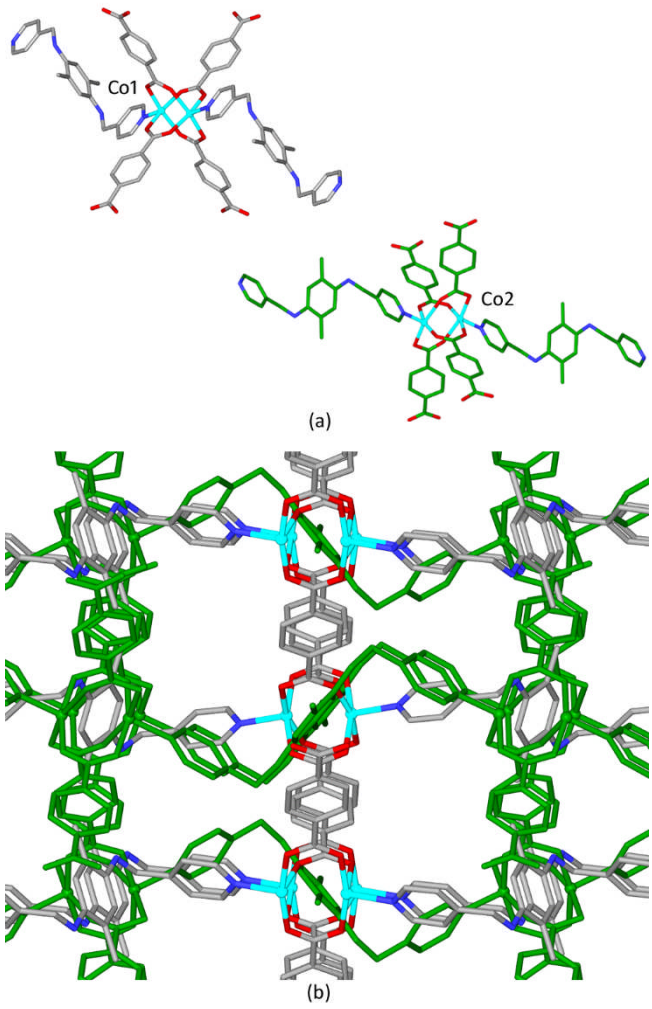


**Figure 2.** Crystal structure of $[Co_2(L1)(bdc)_2]\cdot 2(DMF)$ **β-1(S)**. (a) Highlighting the two structurally distinct paddlewheel moieties with axial L1 ligands; (b) packing diagram with solvent excluded with two structurally distinct **pcu** networks.

whereas the other bridges with one monodentate coordination to one Co(II) (Co-O 2.059(5) Å) and one chelating interaction to the other Co(II) centre (Co-O 2.196(5), 2.352(5) Å). The Co···Co separation within the paddlewheel is 2.8569(16) Å compared with 2.7517(14) Å for **α-1(L)**. The other paddlewheel (Co2, Fig. 3a) is more symmetric with Co-O distances 2.011(4) to 2.163(4) Å and Co···Co separation 2.8015(15) Å. As before, the [Co(bdc)] fragments form a **sql** 2D grid with L1 ligands acting as pillars between these grids. The L1 ligand is ordered (unlike **α-1(L)**) and has a linear conformation. The two independent interpenetrating $[Co_2(L1)(bdc)_2]$ networks form π–π stacking interactions between a $bdc^{2-}$ of one net and phenyl of the other at ring centroid separation 3.591 Å. The channels evident in the structure are more diamond-shaped than rectangular as for **α-1(L)**, Fig. 3b. Solvent-accessible space accounts for 39.3 % of crystal lattice volume. Some solvent positions could be located in the lattice with one water and one DMF position refined. These did not form any

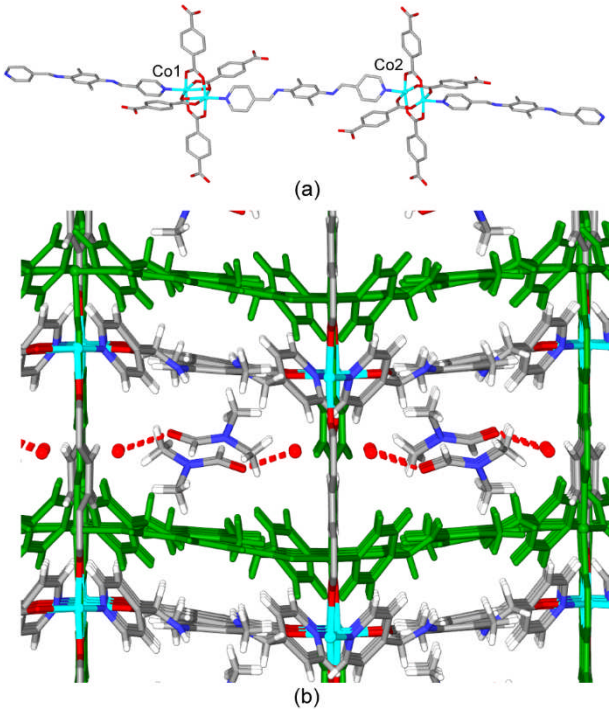


**Figure 3.** Crystal structure of $[Co_2(L1)(bdc)_2]\cdot(H_2O)\cdot(DMF)$ **γ-1(L).** (a) Coordination environment; (b) detail showing rectangular channels with guest molecules.

strong interactions with the MOF framework but hydrogen bond together, Fig. 3. $[Co_2(L1)(bdc)_2]\cdot n(DMF)$ **δ-1(L)** has a large unit cell volume and is again similar to the dominant **α-1(L)** phase. The conformation and level of disorder of the L1 ligand is nearly identical to that in **α-1(L)** however there are differences in the Co(II) coordination environment highlighted in Fig. 4. The $Co_2(O_2CR)_4$ paddlewheel has approximate $C_4$-symmetry with Co-O distances 2.001(3) – 2.059(3) Å giving a more symmetric **sql** grid than was seen for **α-1(L)**. The L1 ligands axial to the paddlewheel show approximate mirror symmetry with respect to one another instead of the approximate $C_2$-symmetry of **α-1(L)**. As before, there are π-π stacking interactions between a $bdc^{2-}$ of one network and dimethylphenyl group of an interpenetrating network with ring centroid separation of 3.55 Å. While the largest channels are of smaller and squarer cross-section than for **δ-1(L)**, the 3D network of channels in **δ-1(L)** actually accounts for more of the unit cell volume at 41.7 %. Residual electron density could not be meaningfully modelled as solvent.

The structure of $[Co_2(L1)_2(bdc)_2]\cdot H_2O$ **2** has the same **pcu** network topology as **1** and is twofold interpenetrating but is not significantly porous. However $Co_2(O_2CR)_4$ paddlewheel motifs are not formed and a mixture of chelating and bridging carboxylate binding is seen, to form a network similar to previously reported materials,[17] Fig. 5 and Fig S28.

Reaction of L1, $Co(NO_3)_2$ and biphenyl-4,4'-dicarboxylic acid ($H_2$bpdc) in a similar manner used for **1** gives $[Co_2(L1)(bpdc)_2]\cdot n(DMF)$ **3** as red block crystals. The structure of

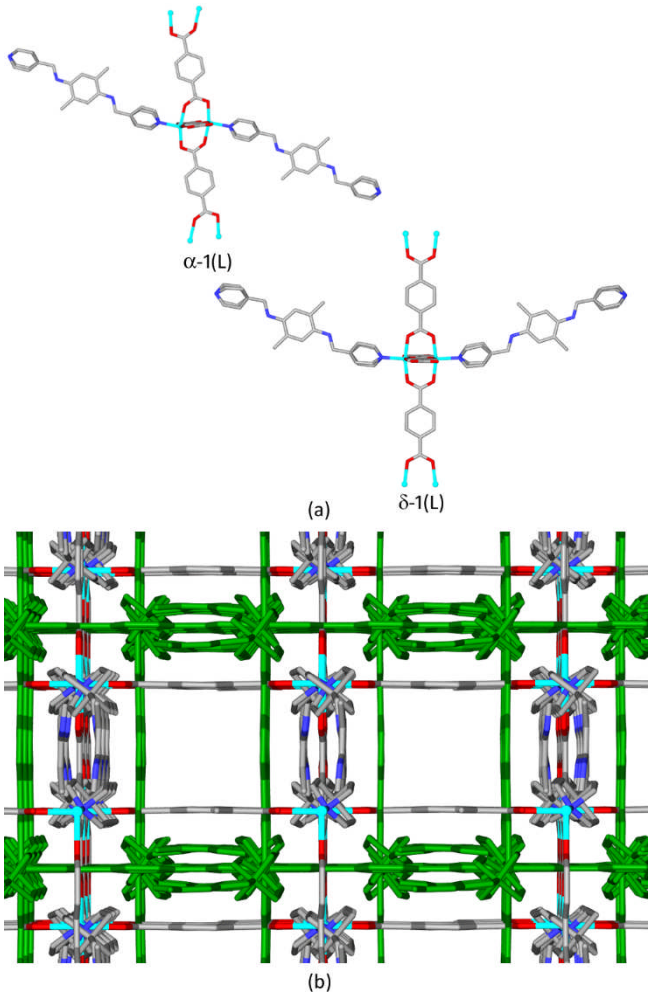


**Figure 4.** Crystal structure of $[Co_2(L1)(bdc)_2]\cdot n(DMF)$ **δ-1(L).** (a) Comparison of coordination environment of this phase with the dominant **α-1(L)** phase; (b) two interpenetrating networks viewed down *c*.

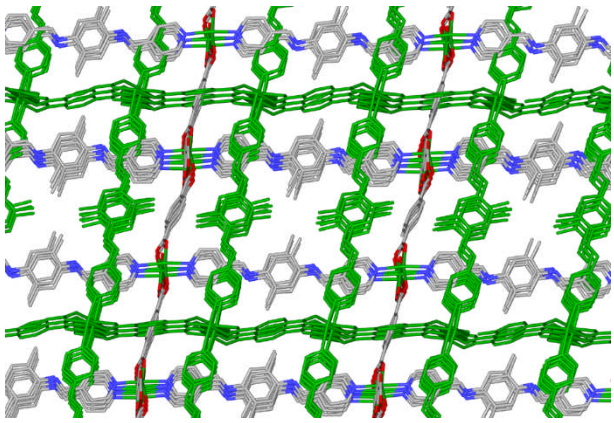

**Figure 5.** Crystal structure of $[Co_2(L1)_2(bdc)_2]\cdot(H_2O))$ **2** with one interpenetrated network in green.

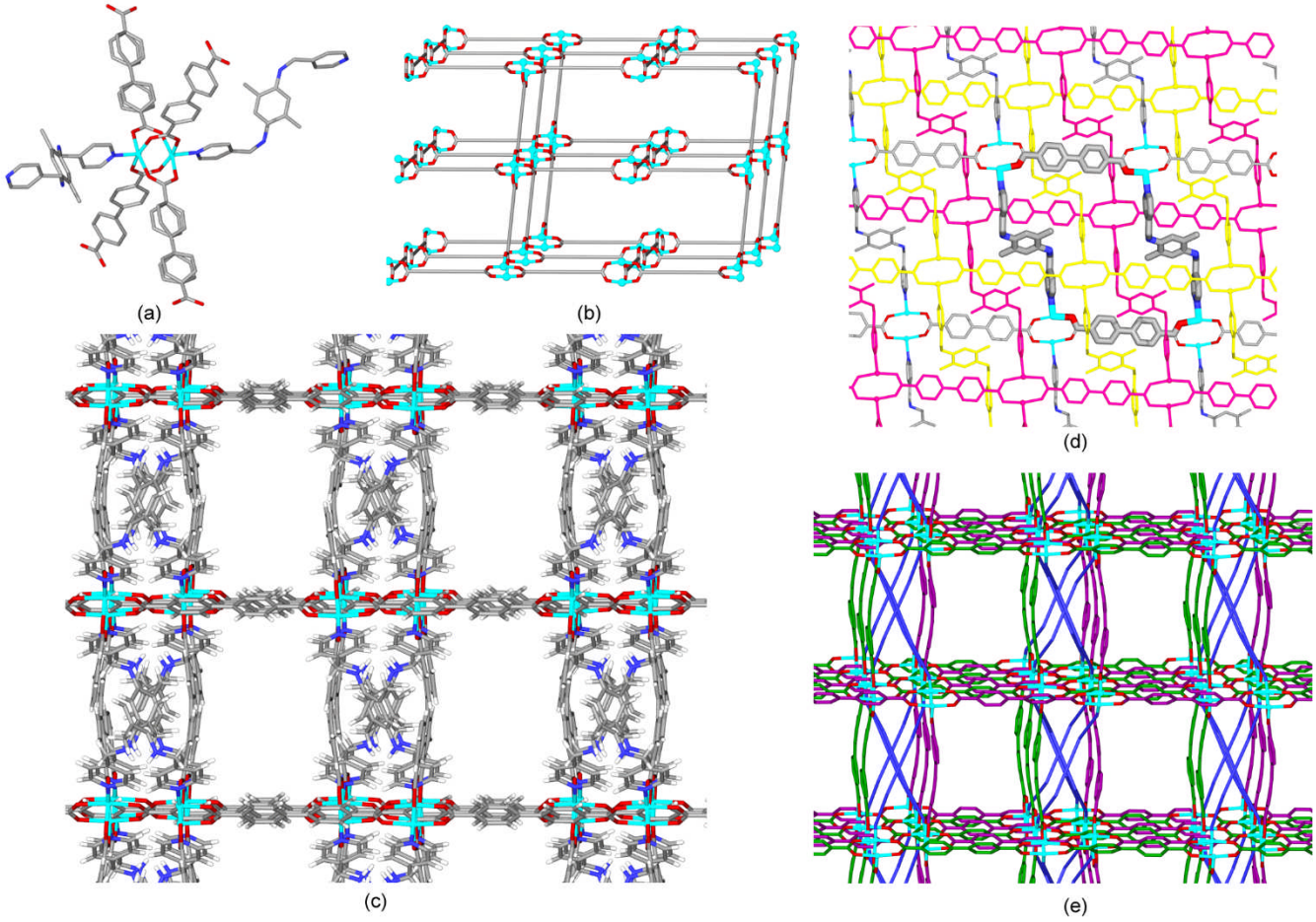


**Figure 6.** Crystal structure of $[Co_2(L1)_2(bpdc)_2]\cdot n(DMF)$ **3**. (a) Coordination environment; (b) [Co(bpdc)] network of **cds** topology with ligands shown schematically; (c) packing diagram viewed down *a* axis, only one position of disordered phenyls are shown; (d) projection in *ab* plane of one set of 3-fold interpenetrating network of $[Co_2(bpdc)(L1)]$ **sql** grid motifs, these are linked by other dpdc2- ligand into 3D self-catenating network; (e) network diagram highlighting the two **cds** networks (one in green, one in purple) linked by L1 ligands shown as blue lines.

$[Co_2(L1)(bpdc)_2]\cdot n(DMF)$ **3** is a MOF with a single self-catenating 3D framework. There are two crystallographically distinct $bpdc^{2-}$ ligands, one of which has disordered phenyl groups. As for **1** a $Co_2(O_2CR)_4$ paddlewheel motif is formed (Co-O distances 2.010(3) – 2.033(3) Å) with axial $bpdc^{2-}$ ligands, Fig. 6a. The $bpdc^{2-}$ ligands bridge to form a network, but here a 3D network of **cds** topology is formed (Fig. 6b) rather than the 2D **sql** net of **1**. There are two **cds** networks in the overall lattice and the L1 ligands link between them to form a single 3D network, Fig 6c. The L1 ligand has an S-configuration with a 85.7 ° angle between the phenyl and pyridyl planes. The network is topologically complex and self-catenates. This is easiest to appreciate by considering the double-tiered layers of composition $[Co_2(bpdc)(L1)]$ that form in the *ab* plane, Fig. 6d. Each layer comprises three interpenetrating grid networks but these are not independent as they are linked together via the $bpdc^{2-}$ ligands that run in the *c* direction, Fig. 6c+e. To the best of our knowledge this 6-connected self-catenating network has not been reported, although other types of self-catenating MOFS with mixed carboxylate/N-donor ligands are known.[18] Rectangular channels are evident viewed down *a* and the solvent accessible void space comprises 34 % of the cell volume. Solvent DMF is contained within the channels (see TGA, Fig. S15) but could not be resolved within the crystal structure.

Both bulk **1** and **3** are porous with BET and Langmuir surface areas 378.1 and 428.1 $m^2\ g^{-1}$ for **1** and 502.3 and 569.2 $m^2\ g^{-1}$ for **3** measured through $N_2$ sorption of activated material. Gas sorption isotherms for $H_2$ are given in Fig. 7 (see Figs. S47-48 for $N_2$, $CO_2$ and $CH_4$). $CO_2$ and $CH_4$ adsorptions are low but both materials display relatively high levels of $H_2$ uptake at 77 *K* at 4.0 mmol $g^{-1}$ (**1**) and 5.1 mmol $g^{-1}$ (**3**) at $p/p_o = 1.0$), with a slight hysteresis for **3**. This is roughly a fifth or a quarter respectively of the $H_2$ uptake seen for NU-100 which is one of the leading MOF hydrogen adsorbers.[19] The MOFs both have pendant amine groups capable of forming hydrogen bonding interactions. Their sorption properties for EtOH – a substrate capable of forming strong hydrogen bonds - were therefore probed. Both materials have high uptake of EtOH at 97.16 $cm^3\ g^{-1}$ at $p/p_o = 0.9$ for **1** and 91.36 $cm^3\ g^{-1}$ for **3** at 298 K. These are relatively high uptakes of EtOH for a MOF or CP,[20] albeit significantly lower than those reported for Cu-BTC,[20b] and a Cu-bipyridinium coordination polymer [20d] at 277 and 164 $cm^3\ g^{-1}$ respectively. Complex **3** shows a simple isotherm but the sorption profile for **1** shows a stepped hysteresis which is indicative of structural changes taking

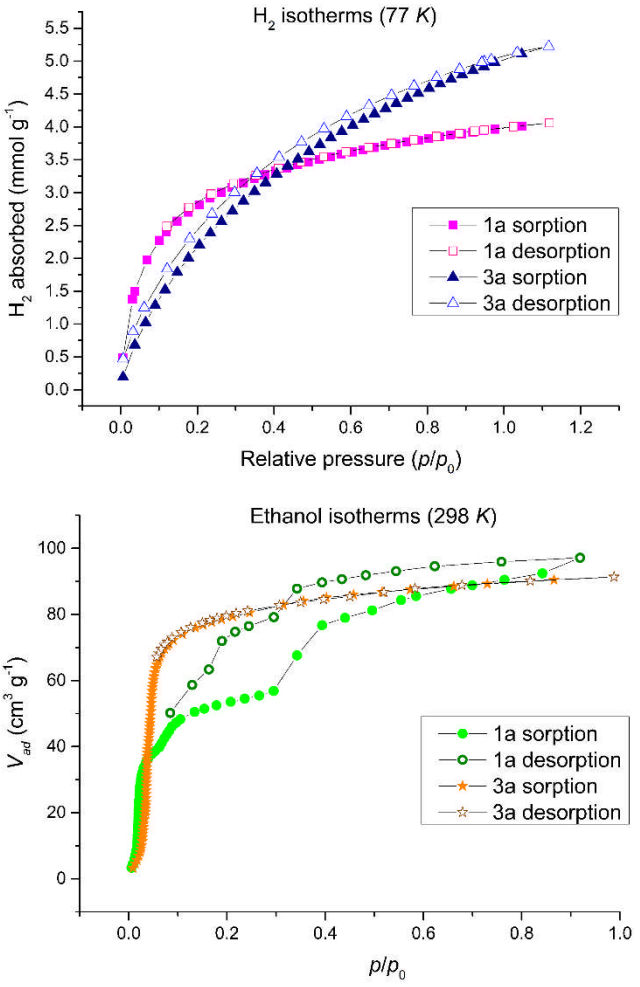


**Figure 7.** $H_2$ (top) and EtOH (bottom) isotherms for bulk **1**[a] and **3**[a]. Materials were washed with acetone, dried under vacuum then activated by heating to 100 °C overnight prior to measurements.

place during the guest up-take, Fig. 7. We investigated this behaviour by single crystal structure determination.

Single crystals of **1** and **3** can be de-solvated then re-solvated with EtOH by immersion in the liquid with retention of sufficient crystallinity for single crystal studies at each stage, with the processes summarised for **1** in Scheme 1. As-synthesised material was washed with acetone to remove DMF, dried under vacuum, and exposed to the atmosphere to give de-solvated or activated material (**#**[a]), then immersed in EtOH to give ethanol solvates (**#**[EtOH]). Uptake of EtOH is accompanied by rapid visible bubbling as atmospheric gases inside the framework are displaced. Powder XRD of **3** (Figs. S45-6) and single crystal studies indicate that complex **3** retains crystallinity and phase purity throughout. This was not the case for bulk **1** which notably loses well-defined crystallinity when removed from mother liquor, with both filtered as-synthesised and acetone/vacuum treated material giving broad and indistinct pXRD patterns (Fig. S43). Nevertheless, fragments of crystalline material could be studied by single crystal diffraction, with determination of a partially de-solvated $[Co_2(L1)(bdc)_2]\cdot 0.5(DMF)\cdot(COMe_2)$ **β-1(S)**[ac] which is a different solvate of **β-1(S)**, and of de-solvated $[Co_2(L1)(bdc)_2]$ **ε-1(L)**, a new phase of **1**. Two structures of ethanol-solvate **1** were also found, one a different solvate of a known phase (also referred to as a pseudopolymorph), namely $[Co_2(L1)(bdc)_2]\cdot n(EtOH)$ **γ-1(L)**[EtOH] and the other a further distinct phase $[Co_2(L1)(bdc)_2]\cdot 2(EtOH)$ **ζ-1(S)**[EtOH].

$[Co_2(L1)(bdc)_2]\cdot 0.5(DMF)\cdot(COMe_2)$ **β-1(S)**[ace] has near identical Co(II) coordination environment and positioning of $bdc^{2-}$ ligands as **β-1(S)** but differs in positioning of solvent molecules and minor differences in rotation of pyridyl rings of L1, Fig. S29. The DMF position is only partly occupied.

In comparison to **α-1(L)** the de-solvated $[Co_2(L1)(bdc)_2]$ **ε-1(L)** sees significant changes to the Co(II) coordination, the rotation of rings within the L1 ligand and manner of separation between the two networks, Fig. 8.[21] The $Co_2(O_2CR)_4$ paddlewheel moiety is skewed with two distinct carboxylate binding modes as was seen for **γ-1(L)**. The L1 ligand has a linear conformation and no disorder of pyridyl groups, and the three arene rings of the ligand are nearly co-planar, with a 17.8 ° angle between phenyl and pyridyl mean planes. It is notable that this ligand conformation has methyl and pyridyl protons effectively shielding the acidic NH groups, rendering them unable to form hydrogen bonding interactions, Fig. 8c. This is not the case for **α-**

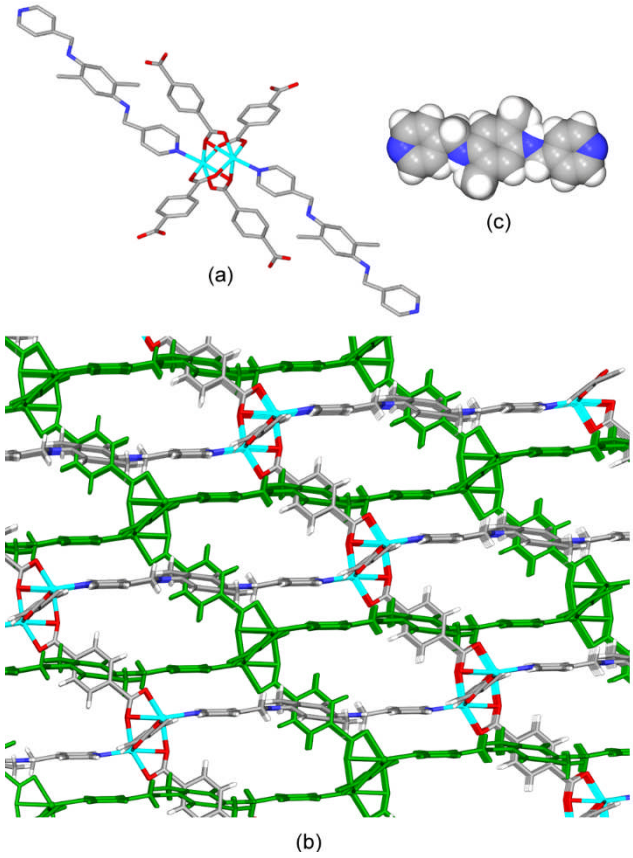


**Figure 8.** Crystal structure of $[Co_2(L1)(bdc)_2]$ **ε-1(L)**. (a) Coordination environment; (b) twofold interpenetrating **pcu** networks; (c) L1 ligand in space filling mode.

**1(L)** nor **γ-1(L)** where the arene groups are substantially twisted from co-planarity (angles between phenyl and pyridyl mean planes of 42.5 and 51.7 ° for **α-1(L)** and 52.6 and 55.5 ° for **γ-1(L)**). The two interpenetrating **pcu** networks of **ε-1(L)** do not form π–π stacking interactions and there is a 5.41 Å ring centroid separation between the L1-phenyl of one network and $bdc^{2-}$ group of another. Hence there is a 1.8 Å relative displacement of the networks in the de-solvated material compared with **α-1(L)**, along with ligand twisting. While rectangular channels are still evident in **ε-1(L)** the solvent-accessible void space has reduced to 34 % of the unit cell volume.

As for the de-solvated or partially de-solvated forms we were able to isolate single crystal fragments of two phases of ethanol solvate of **1**. The structure of the complex $[Co_2(L1)(bdc)_2]\cdot n(EtOH)$ **γ-1(L)$^{EtOH}$** is a pseudopolymorph of **γ-1(L)** with relatively minor structural differences. In **γ-1(L)$^{EtOH}$** both crystallographically different $Co_2(O_2CR)_4$ paddlewheels are significantly skewed with the chelating interactions at Co-O distances 2.069(8), 2.402(8) and 2.069(8), 2.367(8) Å. The L1 ligand is ordered and has a linear conformation. Packing between the networks shows face-to-face π–π stacking interactions between L1-phenyl groups of one network and bdc-phenyl groups of another at ring centroid separations of 3.68 Å, virtually the same as for **α-1(L)**. It is notable that of all the phases and solvates of **1** the conformation of L1 adopted by **γ-1(L)$^{EtOH}$** has the amine NH most accessible for hydrogen bonding interactions, Fig. 9. Ethanol within the channels, however, was too disordered to model.

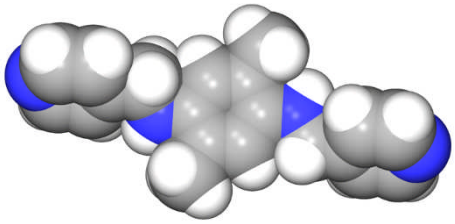

**Figure 9.** Conformation of L1 from crystal structure of $[Co_2(L1)(bdc)_2]\cdot n(EtOH)$ **γ-1(L)$^{EtOH}$** showing open NH groups.

$[Co_2(L1)(bdc)_2]\cdot 2(EtOH)$ **ζ-1(S)$^{EtOH}$** has some structural similarities with **β-1(S)** but is a distinct phase.[21] The complex **ζ-1(S)$^{EtOH}$** is an interpenetrating MOF with two crystallographically-identical **pcu** networks. The $[Co_2(L1)(bdc)_2]$ **pcu** network of **ζ-1(S)$^{EtOH}$** is very similar to the most symmetric of the two types of **pcu** network in **β-1(S)** (Co1 in **β-1(S)** shown in grey in Fig. 2), with S-conformation L1 ligands. The $Co_2(O_2CR)_4$ paddlewheel motif is near $C_4$-symmetric with Co-O distances ranging from 2.0304(19) to 2.0431(19) Å, Fig. 10. The angle between mean planes of pyridyl and phenyl rings of L1 is less acute than for **β-1(S)** at 88.5° giving a slightly longer Co···Co distance between $[Co(bdc)_2]$ layers of 16.6 Å. A comparison of network types in **β-1(S)** and **ζ-1(S)$^{EtOH}$** is given in Fig. 10. For one network type to transform into the other half the L1 ligands would need to invert their S-conformation. Ethanol molecules could be located and form hydrogen bonding interactions with each other inside MOF channels, but do not interact with the amine of L1 which form a

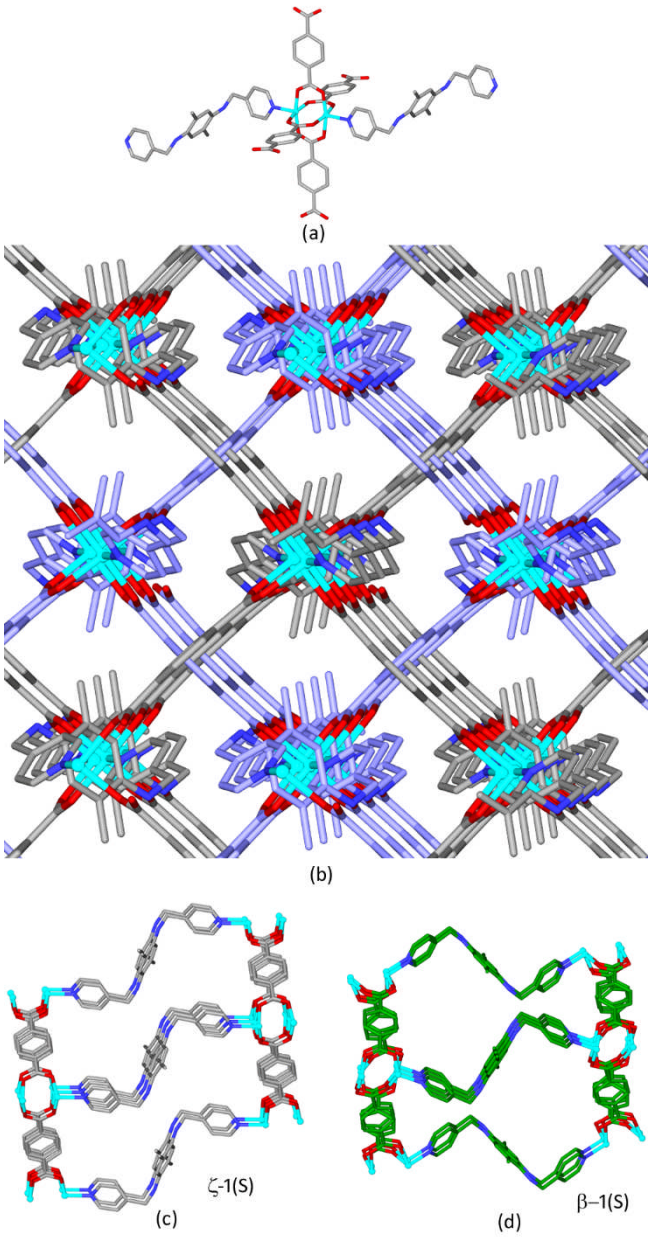


**Figure 10.** Crystal structure of $[Co_2(L1)(bdc)_2]\cdot 2(EtOH)$ **ζ-1(S)$^{EtOH}$** showing (a) coordination environment; (b) packing diagram showing two identical networks interpenetrating; (c) and (d) are a comparison of a single network of **ζ-1(S)$^{EtOH}$** with the structurally distinct single network of **β-1(S)**.

nonconventional NH···π hydrogen bond (N···centroid distance 3.55 Å) to a $bdc^{2-}$ ligand of the interpenetrated network, Fig. S33. This was not observed for **β-1(S)** but a similar interaction occurs between $[Co_2(L1)(bdc)_2]$ networks in **β-1(S)$^{ace}$** (N···centroid distance 3.46 Å).

Synchrotron pXRD pattern was determined for the same sample of bulk type-**1** material that was used for ethanol sorption determination. This material had undergone initial acetone washing and vacuum treatment, then heating at 100 °C under

vacuum, ethanol sorption and desorption, then re-exposure to the atmosphere. The pattern obtained before and after additional vacuum treatment for 2 hr are different indicating the bulk material undergoes structural changes that are not simply solvent-mediated. It is not of high crystallinity, and contains more than one phase that can be attributed to a mixture of linear L1 and S-shaped L1 phases with the latter apparently dominant, Fig. S44. Complex **3**, which has a simple sorption profile for EtOH, does not show significant structural changes neither on de-solvation, high temperature activation, nor on subsequent immersion in EtOH. Complexes $[Co_2(L1)_2(bpdc)_2]$ **3**$^{a}$ and $[Co_2(L1)_2(bpdc)_2]\cdot 1.5(EtOH)$ **3**$^{EtOH}$ have similar unit cell parameters to **3** and all structures were solved in space group *Ccce*. The main discernible difference between the structure of the three materials **3**, **3**$^{a}$ and **3**$^{EtOH}$ is the rotation and degree of disorder of the ligand groups, Fig. 11. Positions of some ethanol molecules in **3**$^{EtOH}$ could be determined, Fig. S39.

As is common for MOF materials, complexes **1** and **3** are not stable in water,[22] collapsing to a largely amorphous material. Crystalline material within the bulk solid of water-decomposed **1** proved to be $L1\cdot H_2O$ (see SI Figs. S19-20 for crystal structure). Interestingly, water-induced decomposition is a relatively slow process for compound **3**. After a week in water, we were able to isolate a fragment of single crystal and determine its structure. Complex $[Co_2(L1)_2(bpdc)_2]\cdot(H_2bpdc)\cdot n(H_2O)$ **3**$^{H2O}$ is isostructural with the other $[Co_2(L1)_2(bpdc)_2]$ materials, with small differences in ligand twisting, Fig. S41. It also exhibited guest up-take in the form of $H_2bpdc$ molecules located inside the channels, Fig. 12. These were presumably released into solution by decomposition of the MOF. Hence this represents a remarkable and rare characterisation of MOF self-cannibalism. This is quite distinct behaviour from major phase changes on water up-take previously reported for other types of twofold interpenetrating pillared MOF materials.[23] The $H_2bpdc$ molecules were refined at half occupancy and form face-to-face $\pi-\pi$ stacking interactions with the ordered $bpdc^{2-}$ ligand (ring centroid separation 3.61 Å). The twist of the phenyl groups of this ligand accommodates this interaction and it is notable that, of all the **3**-series materials, **3**$^{H2O}$ has the most acute angle between phenyl mean planes for this $bpdc^{2-}$ (34.1° *cf.* 37.8-44.07° for the others). Chains of $H_2bdpc$ ligands run along the main channel direction. Repetition of this experiment gave identical results, again with guest $H_2bdpc$ refined to 0.5 occupancy (see Fig. S42).

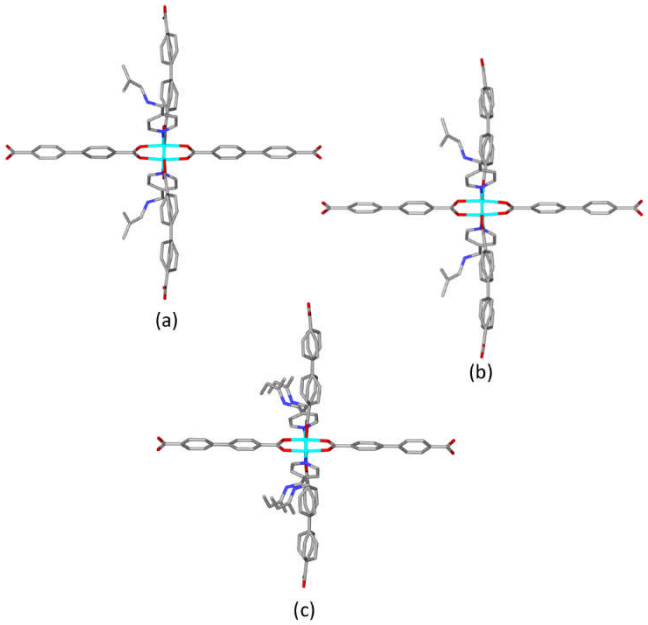


**Figure 11.** Details of crystal structures comparing coordination environments of $[Co_2(L1)_2(bpdc)_2]$ series compounds. (a) **3**; (b) **3**$^{a}$; (c) **3**$^{EtOH}$

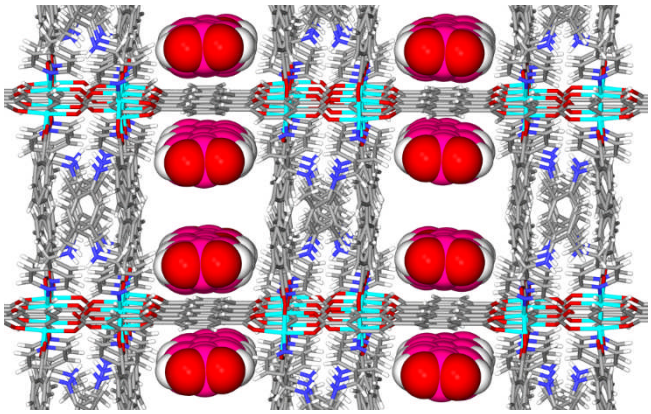

**Figure 12.** Crystal structure of $[Co_2(L1)_2(bpdc)_2]\cdot(H_2bpdc)\cdot n(H_2O)$ **3**$^{H2O}$ with guest $H_2bpdc$ shown in space filling mode in pink.

## Conclusions

Simple ligands have been used to construct new MOF materials with high $H_2$ and EtOH adsorption capability. The conformational flexibility of L1 means that the interpenetrating compound **1** exhibits remarkably complicated phase and structural transformation behaviour which is reflected in the stepped EtOH sorption isotherm. All structural variations of **1** feature twofold interpenetrating pillared layered networks of **pcu** paddlewheel-cluster topology. Structural transformations of solvation changes include commonly observed pathways such as aromatic ring rotations, adjustments to metal coordination environments and slippages between networks, as well as conformational flipping of L1. All observed phases of **1** have significant accessible void space. Aromatic ring rotations of L1 in its more linear conformation open up the accessibility of the NH groups with potential for hydrogen bonding. This, along with gate-opening effects of the more dense phase **ε-1(L)** and conformational flipping of L1 in S-conformation phases may account for the complex isotherm for EtOH adsorption. None of the smaller gases studied can form strong hydrogen bonds and stepped isotherms were not observed. Zaworotko et al recently reported a MOF with highly complex dynamic and multi-responsive flexible behaviour.[11] Interestingly, this is of the same **pcu** structural type as **1** and is also constructed from paddlewheel **sql** grids linked by, in this case rigid, bridging pyridyl ligands. DMOF-1, the prototype for this class of **pcu** frameworks, also shows breathing behaviour.[10]

Complex **3** also has paddlewheel structural motifs and features a single MOF network that is self-catenating in a much more complicated structure than was seen for **1**. The structure can be related to two L1-bridged **cds** networks. Despite its structural complexity, its structural behaviour on solvent de-sorption and sorption is straightforward with no significant changes seen to the network. This may be a function of the additional rigidity of a single network compared with two interpenetrating nets alongside the L1 ligand adopting an S-conformation. MOF **3** is more stable than many in water, though does suffer from hydrolysis typical of many MOF materials. Remarkably, a partially-decomposed material where digested $H_2$bpdc ligand is taken into the MOF channels can be isolated and characterised.

## Experimental Section

**General procedures** Chemicals were obtained from commercial sources and used as received. NMR spectra were recorded on a Bruker DPX 300 MHz NMR spectrometer. ESI-MS were measured on a Bruker Maxis Impact instrument in positive ion mode. Infra-red spectra were recorded as solid phase samples on a Bruker ALPHA Platinum ATR. Elemental analyses were performed by the service at University of Leeds or the London Metropolitan University. Gas and vapour sorption studies were performed on samples from the same batch of compounds **1** and **3**. Samples were washed with acetone, dried under vacuum and then underwent further drying under vacuum at 100 °C overnight immediately prior to measurements. Ethanol sorption was measured at 298 K using a MicrotracBEL Belsorp-Max gas/vapor adsorption measurement instrument. Other gases were measured using a Micromeritics instrument at temperatures indicated.

**Synthesis $N^1$,$N^4$-bis(4-pyridinylmethyl)-2,5-dimethylbenzene-1,4-diamine (L1)** *Step 1:* 4-Pyridinecarboxaldehyde (1.57 g, 14.7 mmol) was dissolved in methanol (40 ml) and added dropwise with stirring to 2,5-dimethyl-benzene-1,4-diamine (1 g, 7.3 mmol) in methanol (40 ml) and heated under reflux for 5 hours at 70 °C. The solvent was evaporated under vacuum to result in a yellow solid product. The product was washed with acetone two times and dried under vacuum to form *N*$^1$,*N*$^4$-bis(4-pyridinylmethylene)-2,5-dimethylbenzene-1,4-diamine (**L1_imine**) (1.9 g, 82.6 %), mpt= 227.5-228 ºC. $^1$H NMR (300 MHz, $CDCl_3$) δ(ppm): δ 8.78 (m, 4H, $Hpy_{ortho}$); 8.43 (s, 2H, H-imine); 7.79 (m, 4H, $Hpy_{meta}$); 6.92 (s, 2H, H-phenyl) and 2.41 (s, 6H, H-methyl); $^{13}$C{$^1$H} NMR (75 MHz, $CDCl_3$) δ (ppm): 156.29, 150.57, 148.35, 143.03, 131.41, 122.19, 119.31 and 17.48. ESI-MS: *m/z* 315.1622 $\{M+H\}^+$ (calc 315.1609). IR (Solid state): υ(cm$^{-1}$) 3056, 2878, 1624, 1594 and 1410. Micro analysis found: C, 75.90; H, 5.80; N, 17.90 %, calculated for $C_{20}H_{18}N_4$: C, 76.41; H, 5.77; N, 17.82 %. *Step 2:* Sodium borohydride (2.5 g, 67 mmol) was added gradually to a pale yellow methanolic solution (250 ml) containing **L1_imine** (1.8 g, 5.7 mmol) at room temperature and left stirring overnight. The solvent was evaporated under vacuum, and the resulted powder was dissolved in deionised water (300 ml) by the addition of aqueous 1M HCl solution. Then, the reaction pH was increased to pH 14 by aqueous 2M sodium hydroxide solution. The ligand was precipitated from the basic solution, filtered, washed by water 4×100 ml and dried under vacuum to result in L1 (1.56 g, 85.71 %), mpt= 186-187 ºC. $^1$H NMR (300 MHz, DMSO-$d_6$) δ(ppm): 8.46 (m, 4H, $Hpy_{ortho}$); 7.33 (m, 4H, $Hpy_{meta}$); 6.12 (s, 2H, H-phenyl); 4.91 (t, 2H, *J*= 6.2 Hz, NH); 4.25 (d, 4H, *J*=5.9 $\underline{CH_2}$-NH), 2.00 (s, 3H, H-methyl); $^{13}$C{$^1$H} NMR (75 MHz, DMSO-$d_6$) δ(ppm): 150.59, 149.31, 136.95, 122.22, 120.32, 113.40, 46.32 and 17.73. ESI-MS: *m/z* 319.1927 $\{M+H\}^+$ (calc 319.1923). IR (Solid state): υ(cm$^{-1}$) 3411, 3071, 2871, 1598, 1524, 1414 and 1361. Micro analysis Found: C, 74.50; H, 6.70; N, 17.20 %, calculated for $C_{20}H_{22}N_4$: C, 75.44; H, 6.96; N, 17.60 %.

**$[Co_2(L1)(bdc)_2]\cdot n(DMF)$ 1** and **$[Co_2(L1)_2(bdc)_2]\cdot H_2O$ 2** A pale yellow solution of L1 (31 mg, 0.1 mmol) and benzene-1,4-dicarboxylic acid ($H_2$bdc, 17 mg, 0.1 mmol) in dimethylformamide (DMF, 4 ml) was added dropwise to $Co(NO_3)_2.6H_2O$ (29 mg, 0.1 mmol) solution in DMF (2 ml). The reaction vial was sealed and placed in the thermal block and heated at 115 °C for 24 hours to give $[Co_2(L1)(bdc)_2]\cdot n(DMF)$ **1** as red block crystals (22 mg, 29 %) and small yellow crystals of $[Co_2(L1)_2(bdc)_2]\cdot H_2O$ **2** (16 mg, 16 %) which were separated by hand prior to analysis and sorption measurements. Crystals of **1** retain single crystallinity after washing with acetone and drying under vacuum, Figure S1. IR (Solid state): υ(cm$^{-1}$) 3431, 3028, 2928, 1671, 1605, 1522, 1384, 551 and 485. Micro analysis found: **1** C, 54.55; H, 4.82; N, 8.29 %, calculated for $[Co_2(L1)(bdc)_2]\cdot DMF\cdot H_2O$: C, 54.75; H, 4.59; N, 8.19 %; **2** C, 57.72; H, 4.55; N, 11.42 %, calculated for $[Co_2(L1)_2(bdc)_2]\cdot 2DMF\cdot 3H_2O$ C, 58.03, H, 5.66, N 10.92.

**$[Co_2(L1)(bpdc)_2]\cdot n(DMF)$ 3** A yellow solution of L1 (31 mg, 0.1 mmol) in DMF (2 ml) and 4,4′-biphenyldicarboxylic acid ($H_2$bpdc) (24 mg, 0.1 mmol) in DMSO (2 ml) was added dropwise to a vial containing $Co(NO_3)_2.6H_2O$ (29 mg, 0.1 mmol) in DMF (2 ml). The reaction vial was sealed and placed in a thermal block and heated at 115 °C for 48 hrs to give red block crystals of $[Co_2(L1)(bpdc)_2]\cdot n(DMF)$ **3** (32 mg, 35.8%). Crystals of **3** retain single crystallinity after washing with acetone and drying under vacuum, Figure S2. IR (Solid state): υ(cm$^{-1}$) 3025, 2925, 1608, 1523, 1391 and 466. Micro analysis found: C, 62.35; H, 4.34; N, 6.14 %, calculated for $[Co_2(L1)(bpdc)_2]$: C, 62.89; H, 4.18; N, 6.11 %.

**Crystallography** Crystals were mounted under inert oil on a MiTeGen tip and flash frozen. X-ray diffraction data were collected using Cu-$K_\alpha$ (λ= 1.54184 Å) or Mo-$K_\alpha$ (λ= 0.71073) radiation using an Agilent Supernova dual-source diffractometer with Atlas S2 CCD detector and fine-focus sealed tube generator, or or using synchrotron radiation (λ= 0.6889 Å) at station I19 of Diamond Light Source, UK. The structures were solved by direct methods using SHELXS or SHELXT and refined by full-matrix on $F^2$ using SHELXL [24] via the Olex2 interface.[25] Further details of crystal structures, data collections and refinements and are given in Tables S1-3 and elsewhere in SI. Crystallographic data in cif format is available at www.ccdc.cam.ac.uk CCDC numbers: L1_imine (1869473), L1 (1869474), L1·$H_2O$ (1869475), **α-1(L)** (1869476), **β-1(S)** (1869477), **γ-1(L)** (1869478), **δ-1(L)** (1869488), **2** (1869479), **ε-1(L)** (1869480), **β-1(S)$^{ace}$** (1869481), **γ-1(L)$^{EtOH}$** (1869482), **ζ-1(S)$^{EtOH}$** (1869483), **3** (1869484), **3$^a$** (1869485), **3$^{EtOH}$** (1869486), **3$^{H2O}$** (1869487). Experimental pXRD patterns were measured on a Bruker Phaser D2 diffractometer using Cu-$K\alpha$ radiation or at SPring-8 BL02B2 Japan at room temperature, λ = 1.000414(2) Å. Calculated patterns were obtained using Mercury.

Data accessibility: data are available at https://doi.org/10.5518/468

## Acknowledgements

We thank the Iraqi Ministry of Higher Education and Scientific Research for studentship (HDJA). This work was further supported by EPRSC (EP/K039202/1, EP/N004884/1), JST CREST (Grant No. JPMJCR13L3), Diamond Light Source (MT-15059) and SPring-8/JASRI (2017B1203). We thank Edward Britton for collecting some X-ray data.

**Keywords:** metal-organic framework • single-crystal-to-single-crystal • hydrogen storage • self-catenating • flexible structure

[1] a) D. J. Tranchemontagne, J. L. Mendoza-Cortés, M. O'Keeffe, O. M. Yaghi, *Chem. Soc. Rev.* **2009**, *38*, 1257-1283; b) J. J. Perry, J. A. Perman, M. J. Zaworotko, *Chem. Soc. Rev.* **2009**, *38*, 1400-1417; c) S. Kitagawa, R. Kitaura, S. Noro, *Angew. Chem. Int. Ed.* **2004**, *43*, 2334-2375; d) R. Robson, *J. Chem. Soc., Dalton Trans.* **2000**, 3735-3744

[2] a) K. Adil, Y. Belmabkhout, R. S. Pillai, A. Cadiau, P. M. Bhatt, A. H. Assen, G. Maurin, M. Eddaoudi, *Chem. Soc. Rev.* **2017**, *46*, 3402-3430; b) A. Schoedel, Z. Ji, O. M. Yaghi, *Nature Energy* **2016**, *1*, 16034; c) Z. R. Herm, E. D. Bloch, J. R. Long, *Chem. Mater.* **2014**, *26*, 323-338; d) J. L. C. Rowsell, O. M. Yaghi, *Angew. Chem. Int. Ed.* **2005**, *44*, 4670-4679.

[3] a) M. Rimoldi, A. J. Howarth, M. R. DeStefano, L. Lin, S. Goswami, P. Li, J. T. Hupp, O. K. Farha, *ACS Catal.* **2017**, *7*, 997-1014; b) S. M. Cohen, Z. Zhang, J. A. Boissonnault, *Inorg. Chem.* **2016**, *55*, 7281-7290; c) J. Liu, L. Chen, H. Cui, J. Zhang, L. Zhang, C.-Y. Su, *Chem. Soc. Rev.* **2014**, *43*, 6011-6061; d) Z.-Y. Gu, J. Park, A. Raiff, Z. Wei, H.-C. Zhou, *ChemCatChem* **2014**, *6*, 67-75; e) J. M. Falkowski, S. Liu, W. Lin, *Isr. J. Chem.* **2012**, *52*, 591-603.

[4] a) J. Della Rocca, D. Liu, W. Lin, *Acc. Chem. Res.* **2011**, *44*, 957-968; b) A. C. McKinlay, R. E. Morris, P. Horcajada, G. Ferey, R. Gref, P. Couvreur, C. Serre, *Angew. Chem. Int. Ed.* **2010**, *49*, 6260-6266.

[5] S. M. Cohen, *Chem. Rev.* **2012**, *112*, 970-1000.

[6] a) A. Halder, D. Ghoshal, *CrystEngComm* **2018**, *20*, 1322-1345; b) R. E. Morris, L. Brammer, *Chem. Soc. Rev.* **2017**, *46*, 5444-5462; c) J.-P. Zhang, P.-Q. Liao, H.-L. Zhou, R.-B. Lin, X.-M. Chen, *Chem. Soc. Rev.* **2014**, *43*, 5789-5814; d) A. Schneemann, V. Bon, I. Schwedler, I. Senkovska, S. Kaskel, R. A. Fisher, *Chem. Soc. Rev.* **2014**, *43*, 6062-6096; e) G. K. Kole, J. J. Vittal, *Chem. Soc. Rev.* **2013**, *42*, 1755-1775; f) S. Kitagawa, R. Matsuda, *Coord. Chem. Rev.* **2007**, *251*, 2490-2509; g) G. A. Halder, C. J. Kepert, *Aust. J. Chem.* **2006**, *59*, 597-604; h) A. J. Fletcher, K. M. Thomas, M. J. Rosseinsky, *J. Solid State Chem.* **2005**, *178*, 2491-2510.

[7] B. F. Abrahams, M. J. Hardie, B. F. Hoskins, R. Robson, G. A. Williams, *J. Am. Chem. Soc.* **1992**, *114*, 10641-10643.

[8] a) C. R. Murdock, B. C. Hughes, Z. Lu, D. M. Jenkins, *Coord. Chem. Rev.* **2014**, *258-259*, 119-136; b) G. Ferey, C. Serre, *Chem. Soc. Rev.* **2009**, *38*, 1380-1399; c) C. Serre, C. Mellot-Draznieks, S. Surblé, N. Audebrand, Y. Filinchuk, G. Férey, *Science* **2007**, *315*, 1828-1831.

[9] recent examples a) Q.-Y. Yang, P. Lama, S. Sen, M. Lusi, K.-J. Chen, W.-Y. Gao, M. Shivanna, T. Pham, N. Hosono, S. Kusaka, J. J. Perry, S. Ma, B. Space, L. J. Barbour, S. Kitagawa, M. J. Zaworotko, *Angew. Chem. Int. Ed.* **2018**, *57*, 5684-5689; b) H.-Y. Yang, Y.-Z. Li, C.-Y. Jiang, H.-H. Wang, L. Hou, Y.-Y. Wang, Z. Zhu, *Cryst. Growth Des.* **2018**, *18*, 3044-3050; c) X. Sun, S. Yao, G. Li, L. Zhang, Q. Huo, Y. Liu, *Inorg. Chem.* **2017**, *56*, 6645-6651.

[10] a) J. S. Grosch, F. Paesani, *J. Am. Chem. Soc.* **2012**, *134*, 4207-4215; b) D. N. Dybtsev, H. Chun, K. Kim, *Angew. Chem. Int. Ed.* **2004**, *43*, 5033-5036; *Angew. Chem.* **2004**, *116*, 5143-5146.

[11] M. Shivanna, Q.-Y. Yang, A. Bajpai, E. Patyk-Kazmierczak, M. J. Zaworotko, *Nature Comm.* **2018**, *9*, 3080.

[12] a) Z. Yin, Y.-L. Zhou, M.-H. Zeng, M. Kurmoo, *Dalton Trans.* **2015**, *44*, 5258-5275; b) H.-Y. Lin, J. Luan, X.-L. Wang, J.-W. Zhang, G.-C. Liu, A.-X. Tian, *RSC Adv.* **2014**, *4*, 62430-62445.

[13] S. Abedi, A. A. Tehrani, H. Ghasempour, A. Morsali, *New. J. Chem.* **2016**, *40*, 6970-6976.

[14] M. Y. Masoomi, S. Beheshti, A. Morsali, *J. Mater. Chem. A* **2014**, *2*, 16863-16866.

[15] For example a) R.-G. Lin, G.-J. Coa, J.-D. Lin, Y.-L. Wang, *New J. Chem.* **2015**, *39*, 9075-9078; b) P. J. Kitson, R. J. Marshall, D. Long, R. S. Forgan, L. Cronin, *Angew. Chem. Int. Ed.* **2014**, *53*, 12723-12728; c) Y. Gong, J. Li, J.-B. Qin, T. Wu, R. Cao, J.-H. Li, *Cryst. Growth Des.* **2011**, *11*, 1662-1674.

[16] For example a) T. Ishiwata, K. Kokado and K. Sada, *Angew. Chem. Int. Ed.* **2017**, *56*, 2608-2612; b) J. M. Seco, S. Pérez-Yánez, D. Briones, J. A. García, J. Cepeda, A. Rodríguez-Diéguez, *Cryst. Grow. Des.* **2017**, *17*, 3893-3906; c) I.-H. Park, K. Kim, S. S. Lee, J. J. Vittal, *Cryst. Growth Des.* **2012**, *12*, 3397-3401; d) J. Li, Y. Peng, H. Liang, Y. Yu, B. Xin, G. Li, Z. Shi, S. Feng, *Eur. J. Inorg. Chem.* **2011**, 2712-2719; e) E.-Y. Choi, K. Park, C.-M. Yang, H. Kim, J.-H. So, S. W. Lee, Y. H. Lee, D. Min, Y.-U. Kwon, *Chem. Eur. J.* **2004**, *10*, 5535-5540.

[17] A. Dey, D. Bairagi, K. Biradha, *Cryst. Growth Des.* **2017**, *17*, 3885-3892.

[18] a) J.-M. Hu, V. A. Blatov, B. Yu, K. Van Hecke, G.-H. Cui, *Dalton Trans.* **2016**, *45*, 2426-2429; b) X.-D. Zhu, Y. Li, W.-X. Zhou, R.-M. Liu, Y.-J. Ding, J. Lü, D. M. Proserpio, *CrystEngComm* **2016**, *18*, 4530-4537; c) Y. Gong, Y. C. Zhou, T. F. Liu, J. Lu, D. M. Proserpio, R. Cao, *Chem. Commun.* **2011**, *47*, 5982-5984; d) L. F. Ma, C. P. Li, L. Y. Wang, M. Du, *Cryst. Growth Des.* **2011**, *11*, 3309-3672; e) L. F. Ma, Q. L. Meng, C. P. Li, B. Li, L. Y. Wang, M. Du, F. P. Liang, *Cryst. Growth Des.* **2010**, *10*, 3036-3043; f) T. Jacobs, R. Clowes, A. I. Cooper, M. J. Hardie *Angew. Chem. Int. Ed.* **2012**, *51*, 5192-5195.

[19] O. M. Farha, A. Ö. Yazaydin, I. Eryazici, C. D. Malliakas, B. G. Hauser, M. G. Kanatzidis, S. T. Nguyen, R. Q. Snurr, J. T. Hupp, *Nat. Chem.* **2010**, *2*, 944-948.

[20] Examples of MOFs with higher EtOH adsorption a) Y. Xiong, Y.-Z. Fan, D. D. Borges, C.-X. Chen, Z.-W. Wei, H.-P. Wang, M. Pan, J.-J. Jiang, G. Maurin, C.-Y. Su, *Chem. Eur. J.* **2016**, *22*, 16147-16156; b) T. R. C. Van Assche, T. Duerinck, J. J. G. Sevillano, S. Calero, G. V. Baron, J. F. M. Denayer, *J. Phys. Chem. C* **2013**, *117*, 18100-18111; c) M. P. Suh, Y. E. Cheon, E. Y. Lee, *Chem. Eur. J.* **2007**, *13*, 4208-4215; d) Q.-Q. Zhang, X.-D. Yang, L. Sun, R.-Y. Guo, M. Chen, J. Zhang, *Inorg. Chem. Commun.* **2018**, *87*, 27-29.

[21] Unit cell checks on over 100 crystals were made on as-synthesised **1** and the same unit cell was not observed.

[22] M. Todaro, G. Buscarino, L. Sciortino, A. Alessi, F. Messina, M. Taddei, M. Ranocchiari, M. Cannas, F. M. Gelardi, *J. Phys. Chem. C* **2016**, *120*, 12879-12889.

[23] D. O'Nolan, A. Kumar, M. J. Zaworotko, *J. Am. Chem. Soc.* **2017**, *139*, 8508-8513.

[24] G. M. Sheldrick, *Acta Crystallogr. A* **2008**, *A64*, 112-122.

[25] O. V. Dolomanov, L. J. Bourhis, R. J. Gildea, J. A. K. Howard, H. Puschmann, *J. Appl. Cryst.* **2009**, *42*, 339-341.